Michigan State University

National Superconducting Cyclotron Laboratory

MANY-BODY COULOMB PERTURBATION OF AZIMUTHAL α–α CORRELATIONS

R. POPESCU, C.K. GELBKE, and T. GLASMACHER

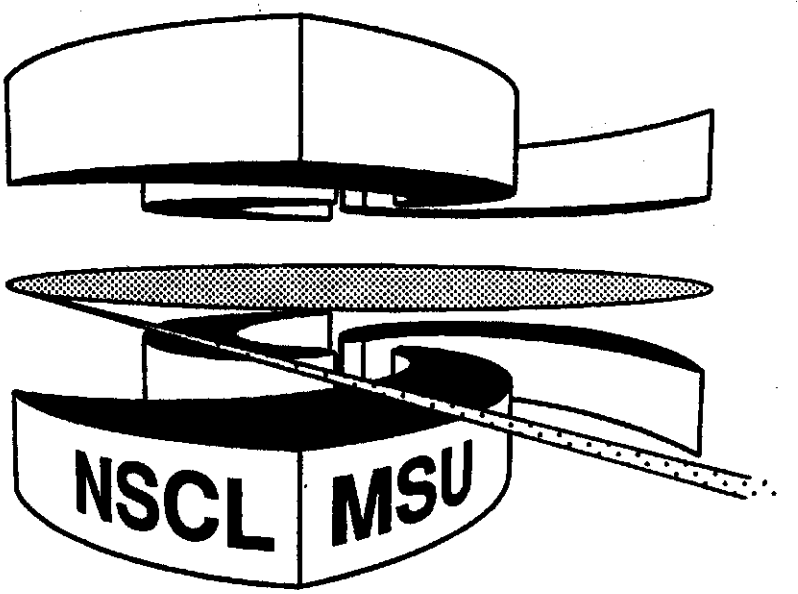

MSUCL-1030

MAY 1996

Many-Body Coulomb Perturbation of Azimuthal α-α Correlations

R. Popescu, C.K. Gelbke, and T. Glasmacher
Department of Physics and Astronomy and National Superconducting Cyclotron Laboratory,
Michigan *State University, East* Lansing, *MI* 48824, *USA*

(May 31, 1996)

The perturbation of azimuthal α-α correlations by many-body Coulomb interactions with other emitted particles is investigated. Individual emissions are simulated by modeling instantaneous emission from the surface of a hot rotating gas. Upon emission, the particle trajectories are calculated by means of classical calculations which incorporate the many-body Coulomb interaction between the emitted particles and the emitting source. For high-multiplicity events, the initial azimuthal correlation between emitted e-particles can be attenuated by final-state Coulomb interactions. The effect is most pronounced for e-particles emitted close to the barrier, but it appears of minor importance for e-particles emitted at large relative angles and at energies well above the Coulomb barrier..

25.70.Pq

I. INTRODUCTION

Particles emitted in intermediate-energy $(E/A \approx 20 - 200MeV)$ heavy-ion collisions are known to exhibit strong azimuthal anisotropies [1–18]. These anisotropies are generally associated with a collective velocity component of the emitted particles with respect to the orientation of the entrance channel reaction plane (defined as the plane perpendicular to the entrance channel orbital angular momentum vector of relative motion). At lower incident energies $(E/A < 100MeV)$ and intermediate impact parameters, the attractive mean field induces collective velocity components which often resemble a rotational motion [l-3,5,6] with a characteristic "V-shaped" azimuthal correlation between the emitted particles [1–4,8–17]. At higher incident energies, the collective motion is dominated by a strong sidewards directed flow caused by the repulsive forces from the pressure in the overlap zone between projectile and target [19–25]. For such emissions, the azimuthal correlations between particles of comparable rapidity are sideways peaked with a maximum at $\Delta\phi = 0$". Often these two types of collective motion coexist [8,10,16–18]. Some additional distortions of the idealized azimuthal anisotropies reflecting only thermal and collective velocity components can arise from final state interactions such as the sequential decay of primary reaction

products produced in particle unbound states [26] or, for small systems, from momentum conservation effects [3,27].

Thermal velocity components decrease for heavier particles, $v_{thermal} \propto m^{-1/2}$, where m is the mass of the emitted particle. In contrast, collective velocity components are independent of the mass of the emitted particles. As a consequence, the effects of collective motion are more pronounced for heavier particles, due to the suppression of "thermal noise". In practice, the effects of collective motion are readily detected in the azimuthal correlations between two emitted α-particles [3,11].

Azimuthal correlations reflecting rotational motion become less pronounced for increasing beam energy and for small-impact parameter collisions [17] selected by cuts on large charged-particle multiplicities, N_C. For truly central collisions of impact parameter $b = 0$, the reaction plane becomes undefined and the azimuthal emission pattern due to collective motion must become isotropic. Thus, a damping of V-shaped azimuthal correlations is qualitatively expected for small impact parameter collisions [17]. More recently, a surprisingly systematic dependence of the azimuthal anisotropies upon the total transverse energy, E_t, of all emitted charged particles has been established [18]. By assuming that E_t provides a measure of the temperature of the reaction zone, $E_t \propto T^{1/2}$, the measured azimuthal anisotropies were found to follow a simple thermal scaling [18].

Decreasing azimuthal anisotropies might, however, also arise from Coulomb distortions in the field of the emitting nucleus and the randomization of the velocity components due to many-body Coulomb interactions between emitted particles. The potential importance of such perturbations has not yet been assessed. In this paper, we investigate this issue via classical many-body Coulomb trajectory calculations for the simple case of an instantaneous release of all emitted particles from the surface of the emitting source using as initial velocity distribution that of a rotating hot gas [3]. We will show that many-body Coulomb perturbations can, indeed, lead to distortions of the azimuthal correlation function. The most important effect is a suppression of the azimuthal correlation function at small relative angles ("Coulomb hole") the magnitude of which carries information about the space-time extent of the emitting system [14,15]. An additional damping of the in-plane to out-of-plane coincidence ratio is predicted for large charged-particle multiplicities, but for the case investigated this damping is of insufficient magnitude to explain the observed [17,18] strong damping of the azimuthal correlations with increasing values of N_C or E_t.

The model assumptions will be presented in Section II, and numerical results will be discussed in Section III. A brief summary will be given in Section IV.

II. PARAMETRIZATION OF INITIAL CONDITIONS.

In order to assess distortions of azimuthal correlation functions by many-body final-state Coulomb interactions we adopt a simple, but well defined classical model [3] for an

instantaneous particle emission from the surface of a sphere containing a hot gas of nucleons and clusters. The parameters of the model are the radius R of the source, its angular velocity ω, and its temperature T. The initial emission pattern from this source is parametrized as [3]

$$\frac{d^5N}{dS \cdot d^3v} \propto (\hat{n} \cdot \vec{v}) \cdot \exp\left\{-\frac{m\left(v^2 - 2R\omega v \sin\theta' \sin\phi' \sin\alpha\right)}{2T}\right\} . \tag{1}$$

Here, v and m denote the velocity and mass of the emitted particle; dS denotes the surface element with normal $\hat{n}$; α is the angle between the axis of rotation $\vec{\omega}$ and the velocity vector $\vec{v}$; θ' and ϕ' denote the polar and azimuthal coordinates of the surface normal $\hat{n}$ for a coordinate system in which the polar (z') axis is parallel to the velocity vector $\vec{v}$ and the plane (x', z') contains the rotation axis $\vec{\omega}$. Our choice of laboratory coordinate system is such that the beam axis is parallel to the z-axis and the angular velocity vector is located in the (x,y)-plane; the reaction plane is defined as the plane perpendicular to $\vec{\omega}$ which contains the beam axis. With this choice of coordinate system,

$$\sin\alpha = \sqrt{1 - \sin^2\theta \sin^2\phi} , \tag{2}$$

where θ is the polar angle of the emitted particle with respect to the beam axis and ϕ is the azimuthal angle, with $\phi = 0°$ or $\phi = 180°$ indicating emission in the reaction plane.

Integration over the surface of the emitting source gives the emission pattern for a rotating classical gas [3],

$$\frac{d^3N}{dE \cdot d\Omega} \propto E \cdot e^{-E/T} \cdot \frac{J_1\left(iA\sqrt{E - E\sin^2\theta \sin^2\phi}\right)}{iA\sqrt{E - E\sin^2\theta \sin^2\phi}} , \tag{3}$$

where J_1 is the first-order Bessel function and

$$A = \sqrt{2m} \cdot \omega R/T . \tag{4}$$

In our simulations, the emission function, Eq. (1), was sampled randomly to generate the initial conditions of the emitted particles. We have chosen source parameters which provide transverse energy spectra and particle distributions which resemble those measured for $^{36}Ar + {}^{197}Au$ collisions at $E/A = 35MeV$ [11,28]. Specifically we used the parameters $R = 10fm$, $\omega R = 0.1c$ and $T = 9MeV$. The element distribution of intermediate mass fragments (IMF: $Z_{IMF} \geq 3$) was assumed to have the probability distribution

$$P(Z_{IMF}) \propto \exp(-0.2Z_{IMF}) . \tag{5}$$

The mass number, A_{IMF}, was assumed to be that of the most abundant isotope of charge number Z_{IMF}. The relative probabilities for light particle emission were chosen according to the ratios [11]

$$P(p)/P(d)/P(t)/P(\alpha) = 2.22/0.86/0.55/2.00\ , \tag{6}$$

and the probability of IMF emission was taken such that

$$\langle N_{IMF} \rangle = 0.143 \cdot N_C - 0.43\ , \tag{7}$$

see also ref. [29]. For $N_C < 4$, we chose $N_{IMF} = 0$.

Calculations were performed for fixed charged particle multiplicity N_C. The initial conditions were generated by randomly sampling the probability distributions, Eqs. (1,5-7). For large particle multiplicities, charge and mass conservation was ensured by rejecting events for which the total emitted charge number, Z_{emit}, was larger than the charge number of the total system, $Z_{tot} = 97$. Because of this charge conservation constraint, the charge distribution of events with large N_C deviates from Eq. (5), falling off more rapidly at high values of Z. For $Z_{emit} < Z_{tot}$, a source residue of charge $Z_{res} = Z_{tot} - Z_{emit}$ was assumed to be formed. Momentum conservation was established by balancing the total momentum of the emitted charged particles, $\mathbf{P}_{emit}$, with the momentum of the remaining system. The mass number of the source residue was taken as $A_{res} = A_{tot} - A_{emit} - N_N$, where A_{emit} is the combined mass number of all emitted charged particles and $N_N = N_C + 10$ is the assumed neutron multiplicity. The source residue's momentum was taken as

$$\mathbf{P}_{res} = -A_{res} \cdot \mathbf{P}_{emit}/(A_{tot} - A_{emit})\ . \tag{8}$$

After having chosen the particles for a given event, their initial positions at the surface of the emitting source and their initial velocities, all particles were assumed to be released at the same time. Their trajectories were then evolved by numerically solving the classical equations of motion under their mutual Coulomb forces. Relativistic effects were neglected. In most calculations, the finite size of the emitted particles was ignored, and the particles were treated as classical point particles. The exclusion of initial conditions in which two particles were separated by a distance less than $d_{min} = 1.2 \cdot (A_1^{1/3} + A_2^{1/3})$ leads to slightly attenuated azimuthal correlations at large multiplicities. To isolate the effects solely due to Coulomb final-state interactions, we ignored this multiplicity-dependent geometrical complication, as well as a possible dependence of the source radius on N_C.

III. RESULTS

In the following, we restrict the discussion to many-body Coulomb distortions calculated for emitted α-particles. This choice was made for the sake of brevity of presentation and justified by the facts that α-particles are emitted with large cross sections and that they are sufficiently heavy to exhibit clear signatures of the underlying collective motion [1–3,5–8,11,12]. Energies and angles of the emitted particles will be given in the center of mass frame of reference. Modifications of single- and two-particle distributions will be discussed in subsections A and B.

A. Single-particle distributions

Energy spectra of α-particles emitted at angular ranges $\theta = 70° - 110°$ and at $\theta = 20° - 60°$, calculated with and without Coulomb final-state interactions, are shown in the top and bottom panels of Fig. 1. The main effect of Coulomb acceleration in the field of the emitting source is a Coulomb-shift of the original energy distribution by the Coulomb barrier $V_C = 27MeV$ towards higher particle energies (compare solid and dotted curves) – justifying, a posteriori, the simple Coulomb-shift approximation used in previous work [3,30]. Many-body Coulomb interactions with other emitted particles, illustrated for the extreme case of $N_C = 40$, significantly modify the low-energy, "sub-barrier" portion of the energy spectrum. In addition, the high-energy tail of the energy spectrum becomes slightly flatter for high-N_C events.

The modification of azimuthal emission patterns with respect to the reaction plane due to finite-size effects is illustrated for $N_C = 20$ in Fig. 2. The figure shows initial (unperturbed) azimuthal distributions of α-particles positioned at the surface of the source by assuming point-particles (curves) or non-overlapping particles of finite size (points: excluded volume assumption). Consideration of excluded volume effects leads to a small multiplicity-dependent flattening of the initial azimuthal distribution. In the following, we adopt the point-particle approximation, primarily in order to avoid a multiplicity-dependent geometrical distortion of the single particle emission pattern unrelated to final-state Coulomb interactions. Together with the other simplifying assumption of instantaneous particle emission, the neglect of excluded volume effects could lead to a slight overestimation of the distortions from many-body Coulomb final-state interactions as compared to a more realistic scenario in which the reaction zone is allowed to evolve dynamically into a possibly non-spherical and/or non-uniform density distribution, and in which particle emission occurs over a finite time interval.

Figures 3 and 4 show energy-integrated azimuthal distributions of α-particles emitted at angular ranges $\theta = 70° - 110°$ and at $\theta = 20° - 60°$, respectively. Because of the $(E \sin^2\theta \sin^2\phi)$-dependence in Eq. (3), emission in the reaction plane is less pronounced at smaller angles than at $\theta = 90°$. In Figs. 3 and 4, solid curves show unperturbed distributions ($N_C = 1$, no Coulomb). The case of maximum Coulomb distortion in the field of the emitting source is represented by dotted curves ($N_C = 1$, with Coulomb). While individual particle trajectories may experience significant deflection in the Coulomb field of the emitting source, the average azimuthal emission pattern exhibits little distortion. For large charged-particle multiplicities $N_C > 20$, the randomizing perturbations due to many-body interactions with the other emitted particles lead to a small flattening of the single-particle azimuthal emission pattern, see dashed and dot-dashed curves for $N_C = 20$ and 40, respectively.

As can be qualitatively expected, many-body Coulomb distortions are more pronounced for particles emitted with lower energy than for particle emitted with higher energy. This

effect is illustrated in Fig. 5. The figure compares unperturbed (curves) and perturbed (for $N_C = 40$, points) azimuthal distributions of α-particles emitted at $\theta = 70° - 110°$ with energies $E_\alpha < E_0$ (open points and dashed curve) and $E_\alpha > E_0$ (solid points and solid curve). In order to account for the acceleration in the Coulomb field of the source, we have taken $E_0 = 30$ and 60 MeV for the unperturbed (no Coulomb) and perturbed (with Coulomb) distributions, respectively. Azimuthal distributions of *energetic* particle thus offer the advantages of enhanced in-plane emission [11] *and* reduced perturbation of this emission pattern from many-body Coulomb interactions.

Figures 6 and 7 show energy integrated and energy-selected azimuthal distributions with respect to the reaction plane of α-particles emitted at $\theta = 70° - 110°$, but for a reduced angular velocity of the emitting source, $\omega R = 0.05c$. The qualitative trends are similar to those established before: Many-body Coulomb perturbations at high charged particle multiplicity, $N_C = 40$, lead to a significant modification of the single-particle emission pattern which is most pronounced for low-energy α-particles and of minor importance for high-energy α-particles.

B. Two-particle correlations

Azimuthal distributions with respect to the true reaction plane, such as those shown in Figs. 3-7, cannot be directly observed because the orientation of the reaction plane cannot be accurately determined on an event-by-event basis. Therefore, measured azimuthal correlations with respect to an experimentally reconstructed reaction plane must be corrected for the resolution with which the reaction plane is determined [11]. Azimuthal two-particle correlation functions exhibit a strong sensitivity to the azimuthal distribution of emitted particles, but they do not require the reconstruction of the reaction plane and allow therefore a more direct comparison between theory and experiment. Beyond their sensitivity to the azimuthal (single-particle) emission pattern, two-particle correlation functions have additional sensitivities to final-state interactions between the two detected particles which depends on the space-time characteristics of the emitting source, see e.g. [15,31–37] and references given there. While this particular aspect is contained in our calculations, we do not explore sensitivities to different space-time characteristics of the emitting source, and refer the reader to the published literature.

Azimuthal correlation functions are defined as the ratio of the two-particle coincidence yield over a suitably chosen background yield, constructed by either the "event-mixing" or "singles" techniques [32,38]. In both techniques, correlations due to enhanced emission in the reaction plane are destroyed for the background events. In analogy, we construct azimuthal two-particle correlation functions from events of fixed charged particle multiplicity according to the definition

$$1 + R(\Delta\phi_{\alpha\alpha}) = C \cdot \frac{\sum_i Y^i_{\alpha\alpha}(\theta_1, \phi_1, \theta_2, \phi_2)}{\sum_{i \neq k} Y^i_\alpha(\theta_1, \phi_1 + \Phi_i) \cdot Y^k_\alpha(\theta_2, \phi_2 + \Phi_k)} \,. \tag{9}$$

In Eq. (9), C is a normalization constant; the labels i and k denote individual events; Φ_i and Φ_k are randomly chosen orientations of the reaction planes for events i and k; sum in the numerator extends over all events i and all coincident pairs of α-particles within a given bin of $\Delta\phi_{\alpha\alpha} = |\phi_1 - \phi_2|$ (defined over the interval $[0°, 180°]$) and selected by specified constraints on E_α and θ. In analogy, the sum in the denominator extends over all pairs of α-particles from different events i and k within the corresponding bin, $\Delta\phi_{\alpha\alpha} = |\phi_1 + \Phi_i - \phi_2 - \Phi_k|$, and selected by the given constraints on E_α and θ. Correlation functions shown in Figs. 8-10 have been normalized by their integral over the interval $\Delta\phi_{\alpha\alpha} \in [90°, 180°]$.

Energy integrated azimuthal two-α-particle correlation functions for $\theta = 70° - 110°$ are shown in Fig. 8. The solid curve shows the initial (unperturbed) correlation function for $N_C = 10$, without final-state interactions. This correlation function exhibits the well known V-shape of the two-particle distribution which arises from the in-plane enhancement of the single-particle emission pattern [3]. The dotted, dashed, and dot-dashed curves show correlation functions modified by many-body final-state Coulomb interactions for $N_C = 10$, 20 and 40, respectively. As expected from Fig. 3, the amplitude of the V-shaped modulation of the correlation function decreases for large values of N_C. In addition, the two-α-particle correlation function exhibits a pronounced minimum at $\Delta\phi_{\alpha\alpha} = 0°$ ("Coulomb hole") which is caused by Coulomb repulsion between the two coincident α-particles. As was already pointed out in refs. [14,15], the magnitude of this minimum depends on the space-time characteristics of the emitting source.

The magnitude and detailed shape of the minimum at $\Delta\phi_{\alpha\alpha} = 0°$ depend on the charged particle multiplicity. This effect is primarily due to the many-body distortion of the single-particle emission pattern with respect to the reaction plane, which leads to a multiplicity-dependent attenuation of the V-shaped azimuthal correlation pattern. Since in the calculations the orientation of the reaction plane is known, this V-shaped "background" pattern can be eliminated by turning off the Φ-randomization in the calculation of the background correlation function. Setting $\Phi_i = \Phi_k = 0°$ in Eq. (9), one can construct a correlation function, $1 + R_{\Phi=0°}(\Delta\phi_{\alpha\alpha})$, for fixed orientation of the reaction plane. This correlation function, shown in Fig. 9, exhibits a clear minimum at $\Delta\phi_{\alpha\alpha} = 0°$ and is flat at large angles, but its shape is rather insensitive to the assumed value of N_C. Such an insensitivity follows from the Koonin-Pratt formula [31–33] which implies that two-particle correlation functions at small relative momenta are sensitive to the space-time geometry of the emitting source, but not to the multiplicity of emitted particles – as long as the correlation function is dominated by the interaction between the two detected particles. The calculated insensitivity of the small-angle behavior of $R_{\Phi=0°}(\Delta\phi_{\alpha\alpha})$ to N_C then indicates that perturbations of the Coulomb hole by interactions with other particles are small.

In the context of small angle correlations, it should be noted that our investigation is

aimed at providing an understanding of the Coulomb modification of large-angle correlation functions. Therefore, the small-angle two-α-particle correlation functions calculated in our Coulomb interaction model are not sufficiently realistic to warrant a direct comparison with experimental data since, for small relative momenta, the experimental two-α-particle correlation function is strongly contaminated by the decay of particle unstable ^8Be nuclei, see e.g. refs. [26,39–41]. Direct comparisons of experimental data and calculations such as ours could, however, be made for correlations between other pairs of particles (such as tritons, ^3He, or IMFs) for which the low-momentum scattering is dominated by the Coulomb force and not by low lying resonances.

In order to summarize the modifications of the two-α-particle azimuthal correlation functions at large angles, we have fit the correlation functions, $1+R(\Delta\phi_{\alpha\alpha})$, by a simple functional form,

$$1 + R(\Delta\phi_{\alpha\alpha}) = a_0(1 + a_2 \cos 2\Delta\phi_{\alpha\alpha}) \ , \tag{10}$$

and constrained the fit to angles $\Delta\phi_{\alpha\alpha} > 45°$. Representative fits are shown in Fig. 10. This figure shows calculated two-α-particle azimuthal correlation functions by points and fits with Eq. (10) by curves. Open and solid points show unperturbed and perturbed correlation functions for $N_C = 40$, respectively, and top and bottom panels show the correlations for the low and high energy cuts used in Fig. 5.

Figure 11 shows the N_C-dependence of the parameter a_2, extracted from the azimuthal correlation functions of two α-particles emitted at $\theta = 70° - 110°$. Circular points show values extracted for energy-integrated correlation functions. Triangle and square shaped points represent results for low ($E_\alpha < E_0$) and high ($E_\alpha > E_0$) energy α-particles, respectively. As before, $E_0 = 30$ and 60 MeV for the cases without and with Coulomb acceleration, respectively. Open and solid points represent unperturbed and perturbed correlations function, respectively. For the cases investigated, the parameter a_2 exhibits a monotonic attenuation as a function of N_C. The relative magnitude of this attenuation is most pronounced for low-energy particles and become insignificant for high-energy particles.

IV. SUMMARY

In summary, we have investigated perturbations of azimuthal emission patterns by many-body final-state Coulomb interactions between emitted particles. The initial positions and momenta of the emitted particles were selected according to a schematic model of instantaneous emission of particles from the surface of a rotating hot gas. Consistent with previous parametrizations [3,30], the acceleration in the Coulomb field of the emitting source was found to produce a shift of the energy spectrum of the emitted particles by the Coulomb energy, V_C, but with little modification of the average azimuthal distribution with respect to the reaction plane. For large charged-particle multiplicities, the randomizing effects of

the many-body final-state Coulomb interactions among the emitted particles lead to a slight broadening of the azimuthal distributions and a related attenuation of the V-shaped azimuthal two-particle correlation functions, characteristic of strong rotational motion. Not surprisingly, this attenuation is more pronounced for particles of low kinetic energy. In addition, the mutual Coulomb interaction between the two detected emitted particles leads to a pronounced minimum of the correlation function at small relative angles (or, more precisely, relative momenta). The precise shape of this minimum was shown [14,15,34] to depend on the size and lifetime of the emitting source.

A quantitative assessment of many-body final-state Coulomb distortions requires knowledge of the initial positions and momenta emitted particles. Since such information is inaccessible to experiment, the quantitative effects of many-body final-state Coulomb interactions can only be evaluated in a given model. Our calculations represent a particularly simple model scenario in which we assumed point-particles, a rather compact initial geometry, and an instantaneous release of all emitted particles. Since less compact source geometries or emission over a larger time interval produce larger inter-particle separations and thus reduced Coulomb interactions, the many-body distortions calculated in this paper may be an overestimate in comparison to a realistic physical situation. The effects are, however, of insufficient magnitude to account for the observed [17,18] rapid attenuation of V-shaped azimuthal two-particle correlations for central collisions selected by high charged particle multiplicities [17] or high transverse energies [18].

We acknowledge stimulating discussions with W.G. Lynch who questioned to which degree azimuthal α-α correlations might be attenuated by many-body Coulomb interactions. This work was supported by the National Science Foundation under Grants No. PHY-9214992 and PHY-95-28844.

---

[1] M.B. Tsang, W.G. Lynch, C.B. Chitwood, D.J. Fields, D.R. Klesch, C.K. Gelbke, G.R. Young, T.C. Awes, R.L. Ferguson, F.E. Obenshain, F. Plasil and R.L. Robinson, Phys. Lett. B **148**, 265 (1984).

[2] M.B. Tsang, C.B. Chitwood, D.J. Fields, C.K. Gelbke, D.R. Klesch, W.G. Lynch, K. Kwiatkowski and V.E. Viola jr., Phys. Rev. Lett. **52**, 1967 (1984).

[3] C.B. Chitwood, D.J. Fields, C.K. Gelbke, D.R. Klesch, W.G. Lynch, M.B. Tsang, T.C. Awes, R.L. Ferguson, F.E. Obenshain, F. Plasil, R.L. Robinson, and G.R. Young, Phys. Rev. C **34**, 858 (1986).

[4] D.J. Fields, W.G. Lynch, T.K. Nayak, M.B. Tsang, C.B. Chitwood, C.K. Gelbke, R. Morse, J. Wilczynski, T.C. Awes, R.L. Ferguson, F. Plasil, F.E. Obenshain, and G.R. Young, Phys.

Rev. C **34**, 536 (1986).

[5] M.B. Tsang, R.M. Ronningen, G. Bertsch, Z. Chen, C.B. Chitwood, D.J. Fields, C.K. Gelbke, W.G. Lynch, T. Nayak, J. Pochodzalla, T. Shea, and W. Trautmann, Phys. Rev. Lett. **57**, 559 (1986).

[6] M.B. Tsang, W.G. Lynch, R.M. Ronningen, Z. Chen, C.K. Gelbke, T. Nayak, J. Pochodzalla, F. Zhu, M. Tohyama, W. Trautmann, and W. Dünnweber, Phys. Rev. Lett. **60**, 1479 (1988).

[7] M.B. Tsang, Y.D. Kim, N. Carlin, Z. Chen, C.K. Gelbke, W.G. Gong, W.G. Lynch, T. Murakami, T. Nayak, R.M. Ronningen, H.M. Xu, F. Zhu, L.G. Sobotka, D.W. Stracener, D.G. Sarantites, Z. Majka, and V. Abenante, Phys. Rev. C **42**, R15 (1990).

[8] W.K. Wilson, W. Benenson, D.A. Cebra, J. Clayton, S. Howden, J. Karn, T. Li, C.A. Ogilvie, A. Vander Molen, G.D. Westfall, J.S. Winfield, B. Young, and A. Nadasen, Phys. Rev. C **41**, R1881 (1990).

[9] D. Ardouin, Z. Basrak, P. Schuck, A. Péghaire, F. Saint-Laurent, H. Delagrange, H. Doubre, C. Grégoire, A. Kyanowski, W. Mittig, J. Péter, Y.P. Viyogi, J. Québert, C.K. Gelbke, W.G. Lynch, M. Maier, J. Pochodzalla, G. Bizard, F. Lefèbvres, B. Tamain, B. Remaud, and F. Sébille, Nucl. Phys. **A514**, 564 (1990).

[10] A. Elmaani, N.N. Ajitanand, J.M. Alexander, R. Lacey, S. Kox, E. Liatard, F. Merchez, T. Motobayashi, B. Noren, C. Perrin, D. Rebreyend, T.U. Chan, G. Anges, and S. Groult, Phys. Rev. C **43**, R2474 (1991).

[11] M.B. Tsang, R.T. de Souza, Y.D. Kim, D.R. Bowman, N. Carlin, C.K. Gelbke, W.G. Gong, W.G. Lynch, L. Phair and F. Zhu, Phys. Rev. C **44**, 2065 (1991).

[12] M.B. Tsang, D.R. Bowman, N. Carlin, C.K. Gelbke, W.G. Gong, Y.D. Kim, W.G. Lynch, L. Phair, R.T. de Souza, and F. Zhu, Phys. Rev. C **47**, 2717 (1993).

[13] S. Wang, Y.Z. Jiang, Y.M. Liu, D. Keane, D. Beavis, S.Y. Chu, S.Y. Fung, M. Vient, C. Hartnack and H. Stöcker Phys. Rev. C **44**, 1091 (1991).

[14] T. Ethvignot, N.N, Ajitanand, J.M. Alexander, E. Bauge, A. Elmaani, L. Kowalski, M. Lopez, M.T. Magda, P. Désesquelles, H. Elhage, A. Giorni, D. Heuer, S. Kox, A. Lleres, F. Merchez, C. Morand, D. Rebreyend, P. Stassi, J.B. Viano, F. Benrachi, B. Chambon, B. Cheynis, D. Drain, and C. Pastor, Phys. Rev. C **46**, 637 (1992).

[15] T. Ethvignot, J.M. Alexander, A.J. Cole, A. Elmaani, P. Désesquelles, H. Elhage, A. Giorni, D. Heuer, S. Kox, A. Lleres, F. Merchez, C. Morand, D. Rebreyend. P. Stassi, J.B. Viano, F. Benrachi, B. Chambon, B. Cheynis, D. Drain, and C. Pastor, Phys. Rev. C **48**, 618 (1993).

[16] R. Lacey, A. Elmaani, J. Lauret, T. Li, W. Bauer, D. Craig, M. Cronqvist, E. Gualtieri, S.

Hannuschke, T. Reposeur, A. Vander Molen, G.D. Westfall, W.K. Wilson, J.S. Winfield, J. Yee, S. Yennello, A. Nadasen, R.S. Tickle, and E. Norbeck, Phys. Rev. Lett. **70**, 1224 (1993).

[17] L. Phair, D.R. Bowman, N. Carlin, C.K. Gelbke, W.G. Gong, Y.D. Kim, M.A. Lisa, W.G. Lynch, G.F. Peaslee, R.T. de Souza, M.B. Tsang, C. Williams, F. Zhu, N. Colonna, K. Hanold, M.A. McMahan, and G.J. Wozniak, Nucl. Phys. **A564**, 453 (1993).

[18] L. Phair, L.G. Moretto, G.J. Wozniak, R.T. de Souza, D.R. Bowman, N. Carlin, C.K. Gelbke, W.G. Gong, Y.D. Kim, M.A. Lisa, W.G. Lynch, G.F. Peaslee, M.B. Tsang, and F. Zhu, to be published.

[19] J.J. Molitoris and H. Stöcker, Phys. Lett. **162B**, 47 (1985).

[20] P. Danielewicz, H. Ströbele, G. Odyniec, D. Bangert, R. Bock, R. Brockmann, J.W. Harris, H.G. Pugh, W. Rauch, R.E. Renfordt, A. Sandoval, D. Schall, L.S. Schröder, and R. Stock, Phys. Rev. C **38**, 120 (1988).

[21] C.A. Ogilvie, D.A. Cebra, J. Clayton, P. Danielewicz, S. Howden, J. Karn, A. Nadasen, A. Vander Molen, G.D. Westfall, W.K. Wilson, and J.S. Winfield, Phys. Rev. C **40**, 2592 (1989).

[22] C.A. Ogilvie, W. Bauer, D.A. Cebra, J. Clayton, S. Howden, J. Karn, A. Nadasen, A. Vander Molen, G.D. Westfall, W.K. Wilson, and J.S. Winfield, Phys. Rev. C **42**, R10 (1990).

[23] J.P. Sullivan, J. Péter, D. Cussol, G. Bizard, P. Brou, M. Louvel, J.P. Patry, R. Regimbart, J.C. Steckmeyer, B. Tamain, E. Crema, H. Doubre, K. Hagel, G.M. Jin, A. Péghaire, F. Saint-Laurent, Y. Cassagnou, R. Legrain, C. Lebrun, E. Rosato, R. McGrath, S.C. Jeong, S.M. Lee, Y. Nagashima, T. Nakagawa, M. Ogihara, J, Kasagi, and T. Motobayashi, Phys. Lett. B **249**, 8 (1990).

[24] W.C. Hsi, G.J. Kunde, J. Pochodzalla, W.G. Lynch, M.B. Tsang, M.L. Begemann-Blaich, D.R. Bowman, R.J. Charity, A. Cosmo, A. Ferrero, C.K. Gelbke, T. Glasmacher, T. Hofmann, G. Immé, I. Iori, J. Hubele, J. Kempter, P. Kreutz, W.D. Kunze, V. Lindenstruth, M.A. Lisa, U. Lynen, M. Mang, A. Moroni, W.F.J. Müller, M. Neumann, B. Ocker, C.A. Ogilvie, G.F. Peaslee, G. Raciti, F. Rosenberger, H. Sann, R. Scardaoni, A. Schüttauf, C. Schwarz, W. Seidel, V. Serfling, L.G. Sobotka, L. Stuttge, S. Tomasevic, W. Trautmann, A. Tucholski, C. Williams, A. Wörner, and B. Zwieglinski, Phys. Rev. Lett. **73**, 3367 (1994).

[25] V. Ramillien, P. Dupieux, J.P. Alard, V. Amouroux, N. Bastid, L. Berger, S. Boussange, L. Fraysse, M. Ibnouzahir, G. Montarou, I. Montbel, P. Pras, Z. Basrak, I.M. Belayev, M. Bini, Th. Blaich, A. Buta, R. Caplar, C. Cerruti, N. Cindro, J.P. Coffin, R. Donà, J. Erö, Z.G. Fan, P. Fintz, Z. Fodor, R. Freifelder, S. Frolov, A. Gobbi, Y. Gregorian, G. Guillaume, C. Hartnack, N. Herrmann, K.D. Hildenbrandt, S. Hölbing, A. Houari, S.C. Jeong, F. Jundt, J. Kecskemeti, P. Koncz, Y. Korchagin,. R. Kotte, M. Krämer, C. Khun, I. Legrand, A. Lebedev, C. Maguire, V. Manko, P. Maurenzig, G. Mgebrishvili, J. Mösner, D. Moisa, W. Neubert, A.

Olmi, G. Pasquali, D. Pelte, M. Petrovici, G. Poggi, F. Rami, W. Reisdorf, A. Sadchikov, D. Schüll, Z. Seres, B. Sikora, V. Simion, S. Smolyankin, U. Sodan, K. Teh, R. Tezkratt, M. Trzaska, M.A. Vasiliev, P. Wagner, J.P. Wessels, T. Wienold, Z. Wilhelmi, D. Wohlfahrth, and A.V. Zhilin, Nucl. Phys. **A587**, 802 (1995).

[26] J. Pochodzalla, C.K. Gelbke, W.G. Lynch, M. Maier, D. Ardouin, H. Delagrange, H. Doubre, C. Grégoire, A. Kyanowski, W. Mittig, A. Péghaire, J. Péter, F. Saint-Laurent, B. Zwieglinski, G. Bizard, F. Lefébvres, B. Tamain, and J. Québert, Y.P. Viyogi, W.A. Friedman, and D.H. Boal, Phys. Rev. C **35**, 1695 (1987).

[27] W.G. Lynch, L.W. Richardson, M.B. Tsang, R.E. Ellis, C.K. Gelbke and R.E. Warner, Phys. Lett. **108B**, 274 (1982).

[28] Y.D. Kim, R.T. de Souza, D.R. Bowman, N. Carlin, C.K. Gelbke, W.G. Gong, W.G. Lynch, L. Phair, M.B. Tsang, and F. Zhu, Phys. Rev. C **45**, 338 (1992).

[29] R.T. de Souza, L. Phair, D.R. Bowman, N. Carlin, C.K. Gelbke, W.G. Gong, Y.D. Kim, M.A. Lisa, W.G. Lynch, G.F. Peaslee, M.B. Tsang, H.M. Xu, F. Zhu, and W.A. Friedman, Phys. Lett. B **268**, 6 (1991).

[30] T.C. Awes, G. Poggi, C.K. Gelbke, B.B. Back, B.G. Glagola, H. Breuer, and V.E. Viola, Jr., Phys. Rev. C **24**, 89 (1991).

[31] S.E. Koonin, Phys. Rev. Lett. **70B**, 43 (1977).

[32] D.H. Boal, C.K. Gelbke, and B.K. Jennings, Rev. Mod. Phys. **62**, 553 (1990).

[33] W. Bauer, C.K. Gelbke, and S. Pratt, Annu. Rev. Nucl. Part. Sci. **42**, 77 (1992).

[34] Y.D. Kim, R.T. de Souza, C.K. Gelbke, W.G. Gong, and S. Pratt, Phys. Rev. C **45**, 387 (1992).

[35] T. Glasmacher, L. Phair, D.R. Bowman, C.K. Gelbke, W.G. Gong, Y.D. Kim, M.A. Lisa, W.G. Lynch, G.F. Peaslee, R.T. de Souza, M.B. Tsang, and F. Zhu, Phys. Rev. C **50**, 952 (1994).

[36] T. Glasmacher, C.K. Gelbke, and S. Pratt, Phys. Lett. B **314**, 265 (1993).

[37] E. Cornell, T.M. Hamilton, D. Fox, Y. Lou, R.T. de Souza, M.J. Huang, W.C. Hsi, C. Schwarz, C. Williams, D.R. Bowman, J. Dinius, C.K. Gelbke, T. Glasmacher, D.O. Handzy, M.A. Lisa, W.G. Lynch, G.F. Peaslee, L. Phair, M.B. Tsang, G. VanBuren, R.J. Charity, L.G. Sobotka, and W.A. Friedman, Phys. Rev. Lett. **75**, 1475 (1995).

[38] M.A. Lisa, W.G. Gong, C.K. Gelbke, and W.G. Lynch, Phys. Rev. C **44**, 2865 (1991).

[39] Z. Chen, C.K. Gelbke, W.G. Gong, Y.D. Kim, W.G. Lynch, M.R. Maier, J. Pochodzalla, M.B.

Tsang, F. Saint-Laurent, D. Ardouin, H. Delagrange, H. Doubre, J. Kasagi, A. Kyanowski, A. Péghaire, J. Péter, E. Rosato, G. Bizard, F. Lefébvres, B. Tamain, J. Québert, and Y.P. Viyogi, Phys. Rev. C **36**, 2297 (1987).

[40] G.J. Kunde, J. Pochodzalla, J. Aichelin, E. Berdermann, B. Berthier, C. Cerruti, C.K. Gelbke, J. Hubele, P. Kreutz, S. Leray, R. Lucas, U. Lynen, U. Milkau, W.F.J. Müller, C. Ngô, C.H. Pinkenburg, G. Raciti, H. Sann, and W. Trautmann, Phys. Lett. B **272**, 202 (1991).

[41] C. Schwarz, W.G. Gong, N. Carlin, C.K. Gelbke, Y.D. Kim, W.G. Lynch, T. Murakami, G. Poggi, R.T. de Souza, M.B. Tsang, H.M. Xu, D.E. Fields, K. Kwiatkowski, V.E. Viola jr., and S.J. Yennello, Phys. Rev. C **48**, 676 (1993).

FIG. 1. Energy spectra of α-particles emitted at $\theta = 70°-110°$ (upper panel) and at $\theta = 20°-60°$ (lower panel). Dot-dashed curves show energy distributions without Coulomb interactions, and solid curves show these spectra shifted by the Coulomb energy, $V_C = 27MeV$. Dotted curves illustrate the modification by Coulomb repulsion from the source, assuming $N_C = 1$, and dashed curves illustrate the effect of many-body final state interactions for $N_C = 40$.

FIG. 2. Curves and points compare the initial azimuthal distributions of α-particles emitted at $\theta = 70° - 110°$ for the emission of $N_C = 20$ point-particles and for the emission of $N_C = 20$ non-overlapping, finite-size particles (excluded volume effect), respectively. Solid curve and solid points show energy-integrated distribution, dashed and dotted curves and open points show distributions for the indicated energy cuts.

FIG. 3. Energy integrated azimuthal distribution with respect to the reaction plane for α-particles emitted at $\theta = 70°-110°$. The solid curve shows the unperturbed distribution ($N_C = 1$, no Coulomb); the dotted curve ($N_C = 1$, with Coulomb) illustrates the distortion in the Coulomb field of the source ($Z_{res} = 95$). The dashed and dot-dashed curves illustrate many-body distortions for $N_C = 20$ and 40, respectively.

FIG. 4. Energy integrated azimuthal distribution with respect to the reaction plane for α-particles emitted at $\theta = 20° - 60°$. The solid curve shows the unperturbed distribution ($N_C = 1$, no Coulomb); the dotted curve ($N_C = 1$, with Coulomb) illustrates the distortion in the Coulomb field of the source ($Z_{res} = 95$). The dashed and dot-dashed curves illustrate many-body distortions for $N_C = 20$ and 40, respectively.

FIG. 5. Azimuthal distribution with respect to the reaction plane for α-particles emitted at $\theta = 70° - 110°$. The solid (open) points and solid (dashed) curve show distributions for high, $E_\alpha > E_0$, (low, $E_\alpha < E_0$) energy α-particles, respectively. Curves show unperturbed distributions ($N_C = 1$, no Coulomb); points show distortions for $N_C = 40$.

FIG. 6. Energy integrated azimuthal distribution with respect to the reaction plane for α-particles emitted at $\theta = 70° - 110°$, for a reduced angular velocity of the emitting system ($\omega R = 0.05c$). The solid curve shows the unperturbed distribution ($N_C = 1$, no Coulomb); the dotted curve ($N_C = 1$, with Coulomb) illustrates the distortion in the Coulomb field of the source ($Z_{res} = 95$). The dashed and dot-dashed curves illustrate many-body distortions for $N_C = 20$ and 40, respectively.

FIG. 7. Azimuthal distribution with respect to the reaction plane for α-particles emitted at $\theta = 70° - 110°$, but for a reduced angular velocity of the emitting system ($\omega R = 0.05c$). The solid (open) points and solid (dashed) curve show distributions for high, $E_\alpha > E_0$, (low, $E_\alpha < E_0$) energy α-particles, respectively. Curves show unperturbed distributions ($N_C = 1$, no Coulomb); points show distortions for $N_C = 40$.

FIG. 8. Energy integrated azimuthal two-α-particle correlation functions, $1 + R(\Delta\phi_{\alpha\alpha})$, for α-particles emitted at $\theta = 70° - 110°$. The solid curve shows the unperturbed correlation function for $N_C = 10$. The dotted, dashed, and dot-dashed curves show correlation functions modified by many-body final-state Coulomb interactions for $N_C = 10$, 20, and 40, respectively.

FIG. 9. Energy integrated correlation function, $1 + R_{\Phi=0°}(\Delta\phi_{\alpha\alpha})$, for fixed orientation of the reaction plane and for α-particles emitted at $\theta = 70° - 110°$. The solid, dotted, and dashed curves show correlation functions modified by many-body final-state Coulomb interactions for $N_C = 10$, 20, and 40, respectively.

FIG. 10. Azimuthal two-α-particle correlation functions for $N_C = 40$ and for α-particles emitted at $\theta = 70° - 110°$. Open and solid points show unperturbed and perturbed correlation functions, respectively. The top and bottom panels show the correlations for low ($E_\alpha < E_0$) and high ($E_\alpha > E_0$) energy α-particles, respectively. Curves show fits with Eq. (10) as discussed in the text.

FIG. 11. Dependence of the parameter a_2 on the charged-particle multiplicity N_C extracted from fitting azimuthal two-α-particle correlation functions, $1 + R(\Delta\phi_{\alpha\alpha})$, for α-particles emitted at $\theta = 70° - 110°$. Open and solid points represent values extracted from fits to unperturbed and perturbed correlation functions. Circular points show values extracted for energy-integrated correlation functions. Triangle and square shaped points represent results for low ($E_\alpha < E_0$) and high ($E_\alpha > E_0$) energy α-particles, respectively.

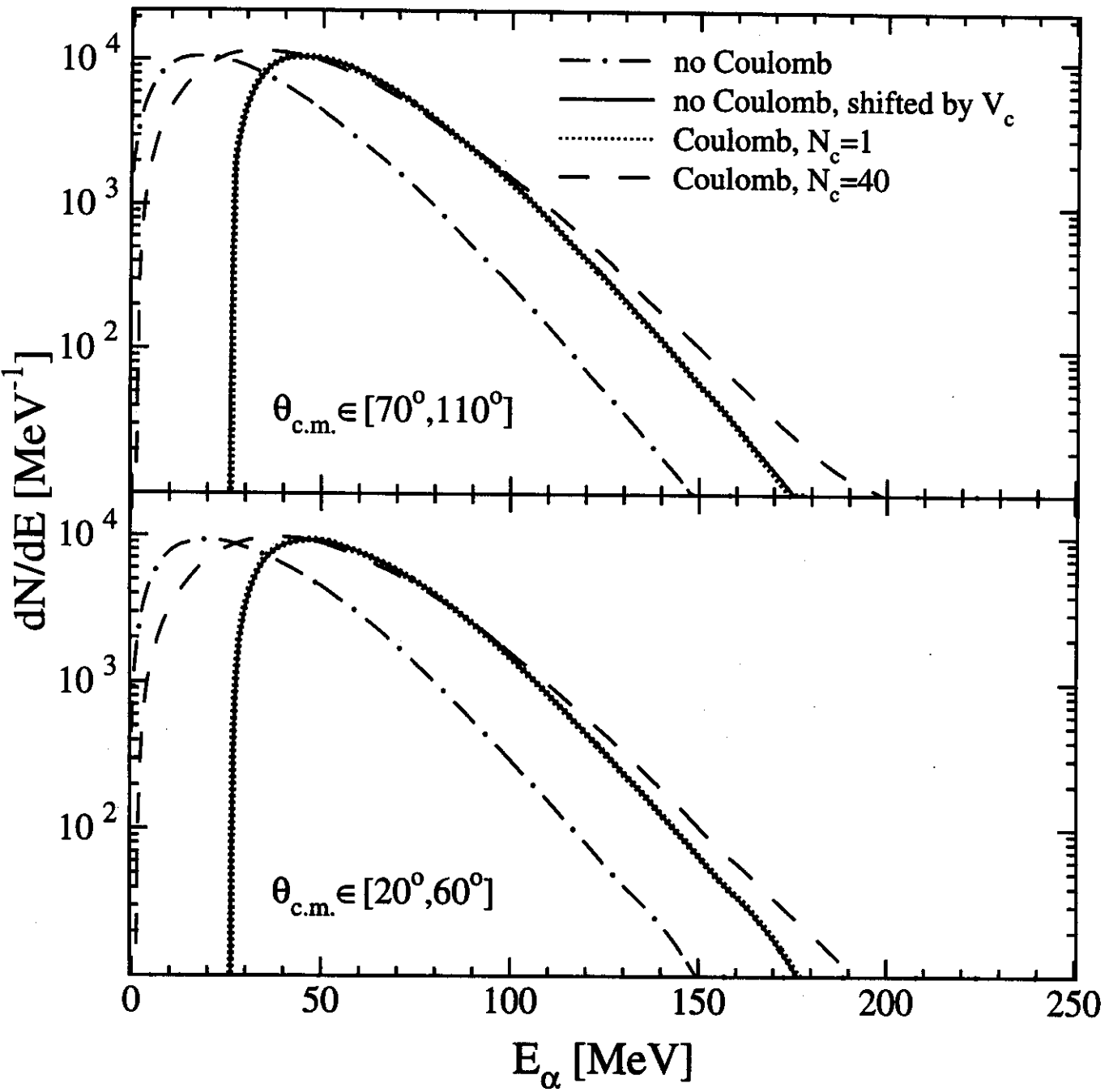
no Coulomb
no Coulomb, shifted by V_c
Coulomb, N_c=1
Coulomb, N_c=40
$\theta_{c.m.} \in [70^o,110^o]$
$\theta_{c.m.} \in [20^o,60^o]$
dN/dE [MeV^{-1}]
E_α [MeV]
10^4
10^3
10^2
0
50
100
150
200
250

Fig. 1

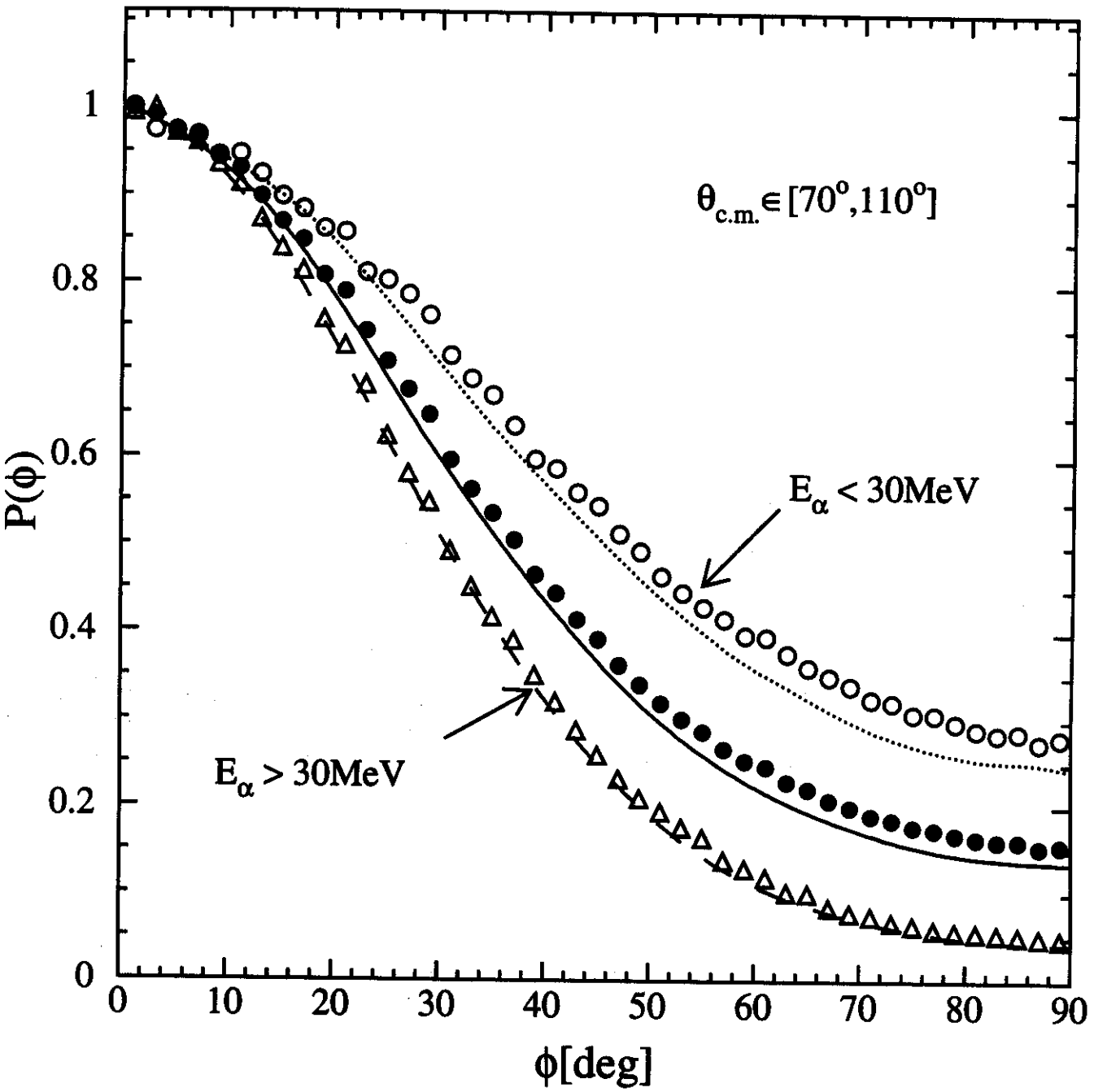
1
0.8
0.6
0.4
0.2
0
P(ϕ)
0
10
20
30
40
50
60
70
80
90
ϕ[deg]
θc.m.∈[70°,110°]
Eα < 30MeV
Eα > 30MeV

Fig. 2

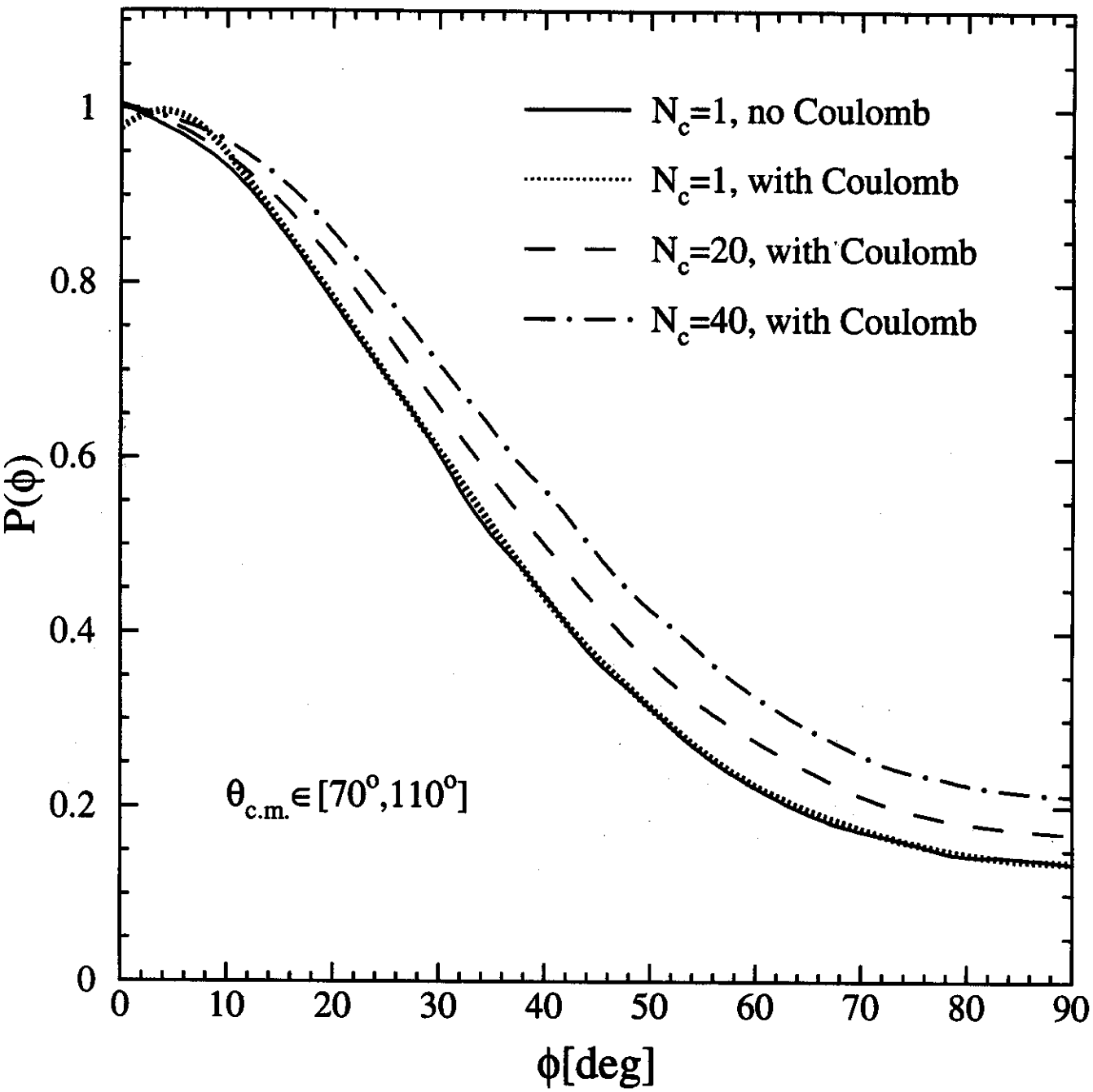
1
0.8
0.6
0.4
0.2
0
P(φ)
0
10
20
30
40
50
60
70
80
90
φ[deg]
N_c=1, no Coulomb
N_c=1, with Coulomb
N_c=20, with Coulomb
N_c=40, with Coulomb
θ_c.m.∈[70°,110°]

Fig. 3

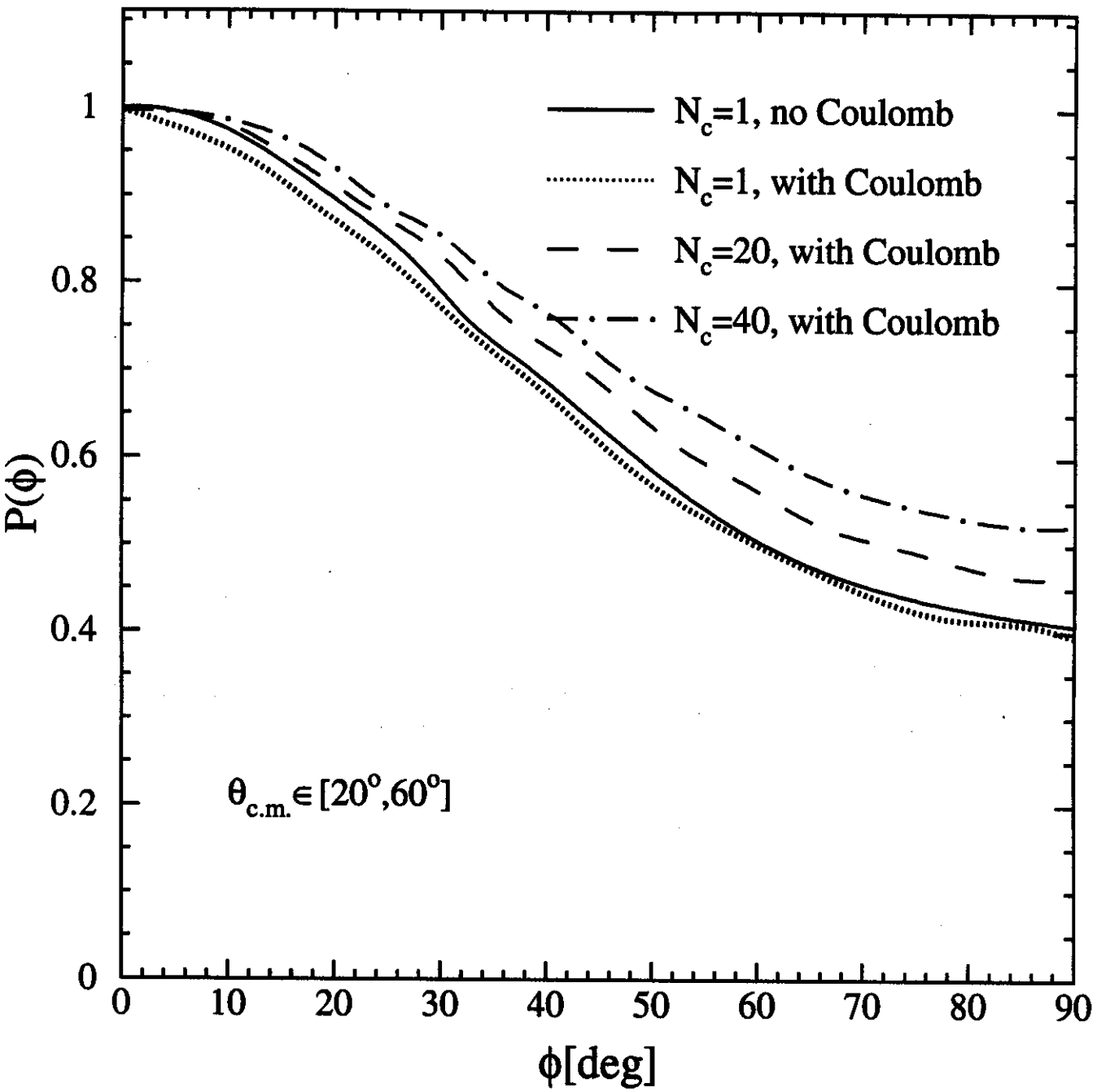
1
0.8
0.6
0.4
0.2
0
P(ϕ)
0
10
20
30
40
50
60
70
80
90
ϕ[deg]
N_c=1, no Coulomb
N_c=1, with Coulomb
N_c=20, with Coulomb
N_c=40, with Coulomb
θ_c.m. ∈ [20°,60°]

Fig. 4

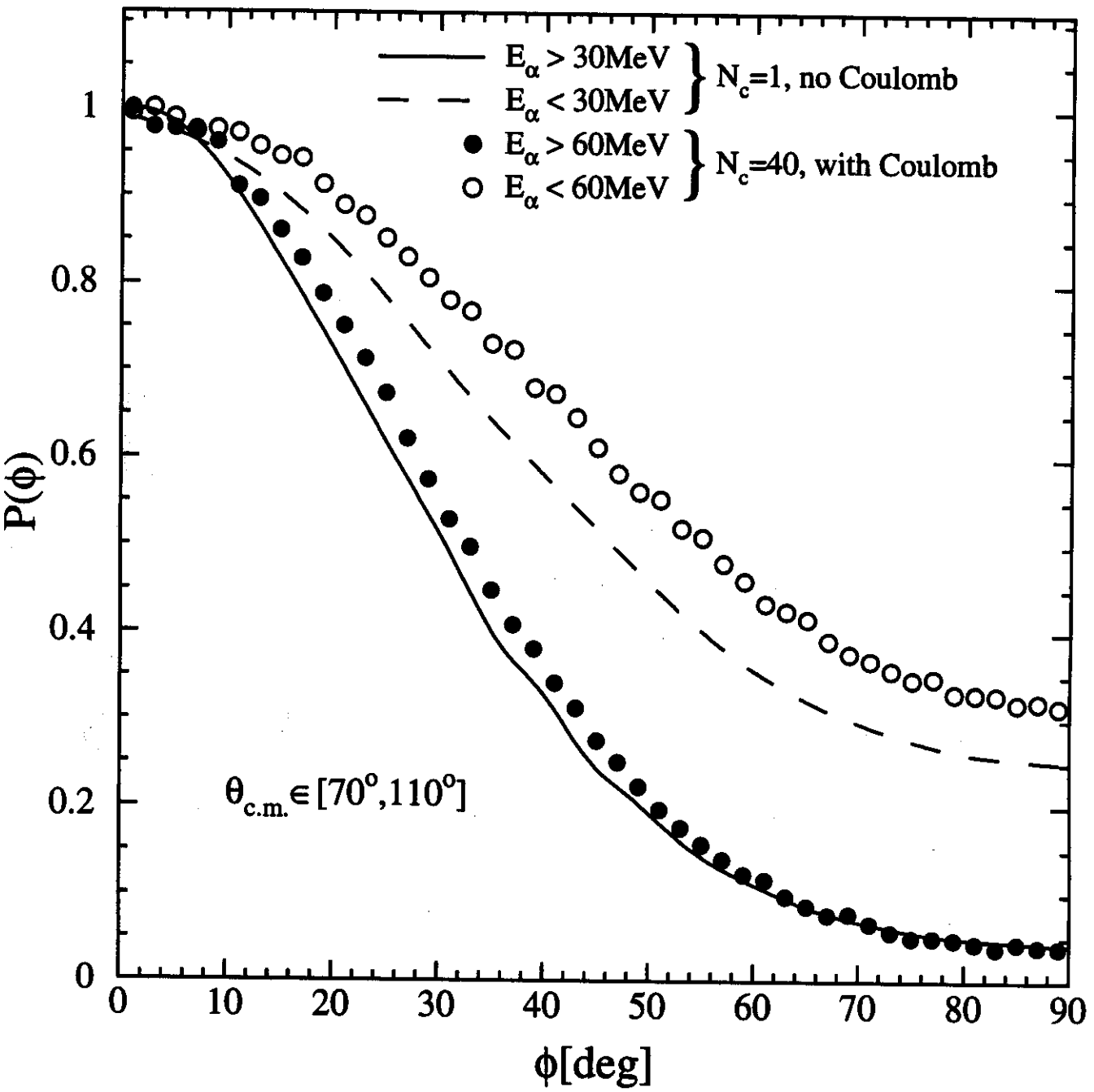
$E_\alpha > 30MeV$
$E_\alpha < 30MeV$
N_c=1, no Coulomb
$E_\alpha > 60MeV$
$E_\alpha < 60MeV$
N_c=40, with Coulomb
$\theta_{c.m.} \in [70^o, 110^o]$
P(ϕ)
ϕ[deg]
0
0.2
0.4
0.6
0.8
1
0
10
20
30
40
50
60
70
80
90

Fig. 5

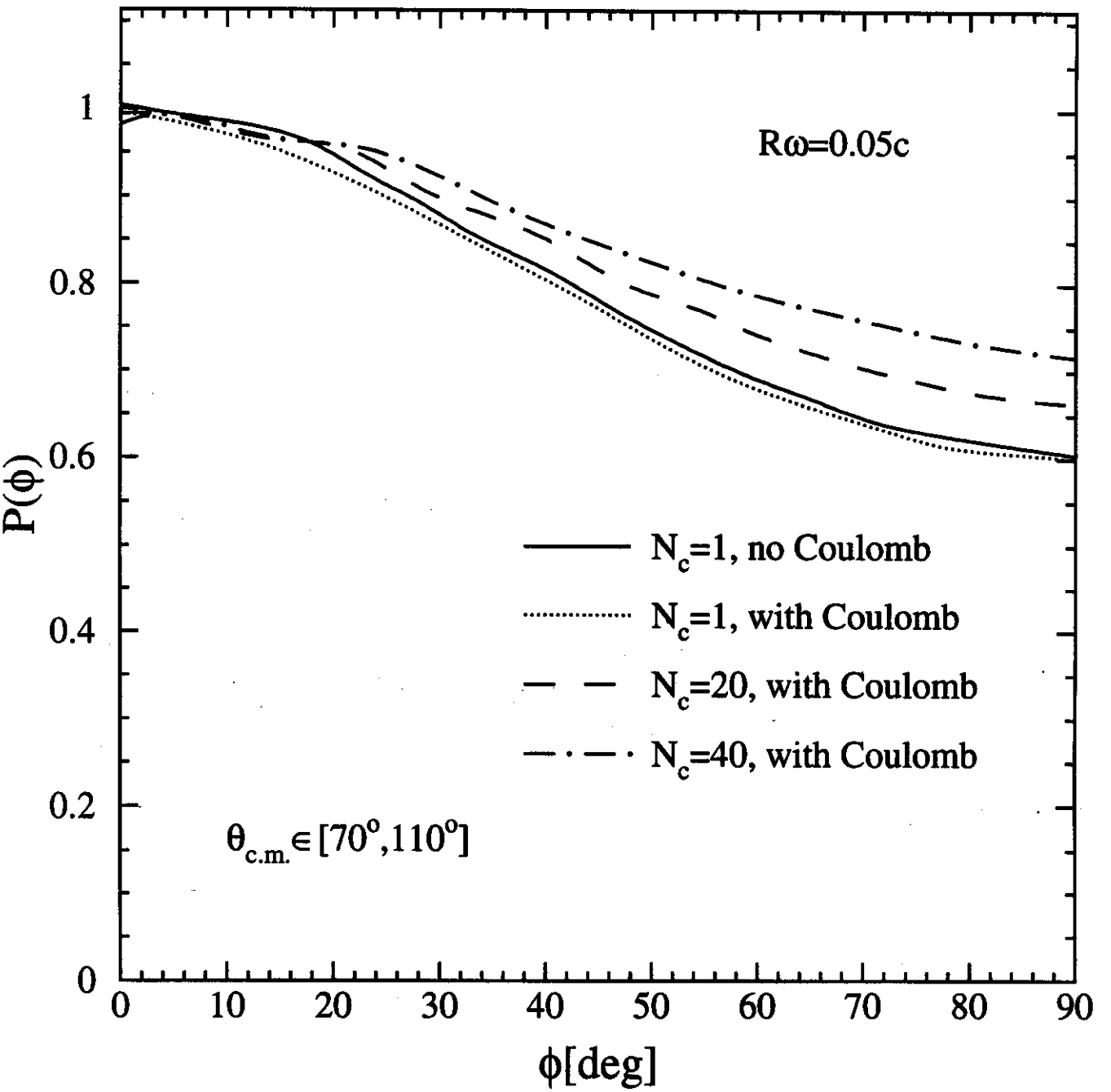
1
0.8
0.6
0.4
0.2
0
P(ϕ)
Rω=0.05c
N_c=1, no Coulomb
N_c=1, with Coulomb
N_c=20, with Coulomb
N_c=40, with Coulomb
θ_c.m.∈[70°,110°]
0
10
20
30
40
50
60
70
80
90
ϕ[deg]

Fig. 6

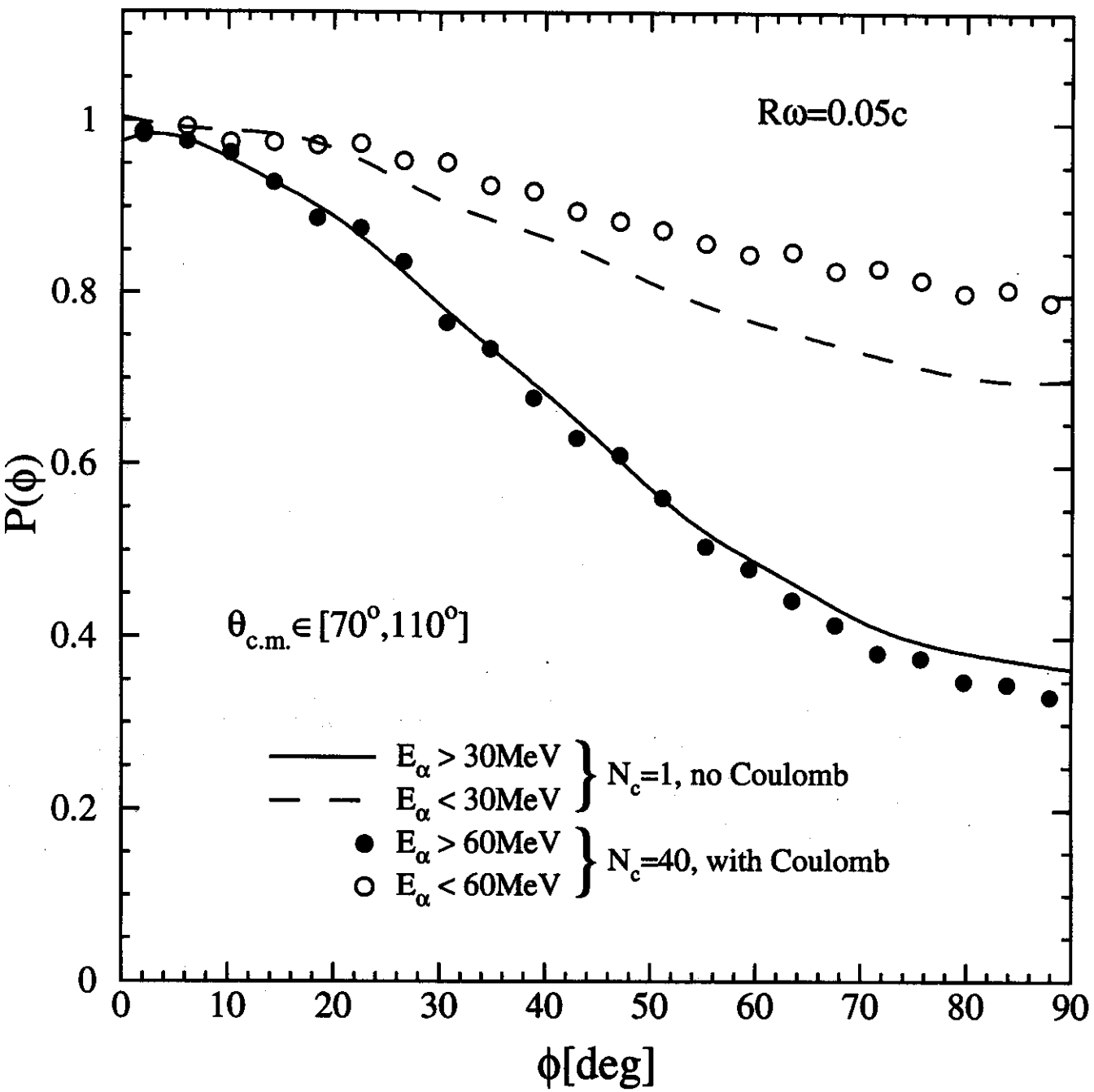
Rω=0.05c
θc.m.∈[70°,110°]
Eα > 30MeV
Eα < 30MeV
Nc=1, no Coulomb
Eα > 60MeV
Eα < 60MeV
Nc=40, with Coulomb
P(φ)
φ[deg]
0
0.2
0.4
0.6
0.8
1
0
10
20
30
40
50
60
70
80
90

Fig. 7

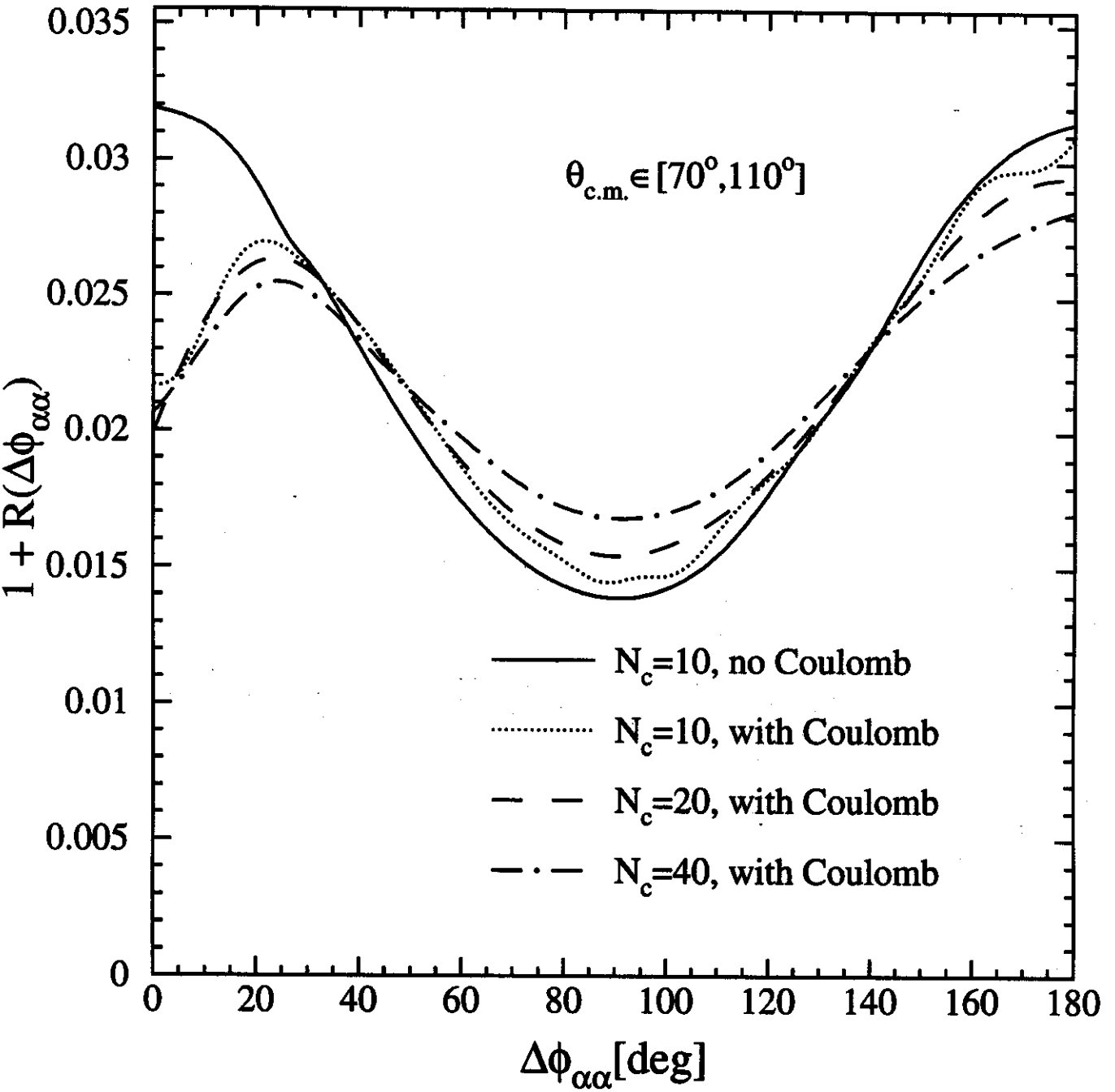
0.035
0.03
0.025
0.02
0.015
0.01
0.005
0
0
20
40
60
80
100
120
140
160
180
$1 + R(\Delta\phi_{\alpha\alpha})$
$\Delta\phi_{\alpha\alpha}$[deg]
$\theta_{c.m.} \in [70^o, 110^o]$
N_c=10, no Coulomb
N_c=10, with Coulomb
N_c=20, with Coulomb
N_c=40, with Coulomb

Fig 8

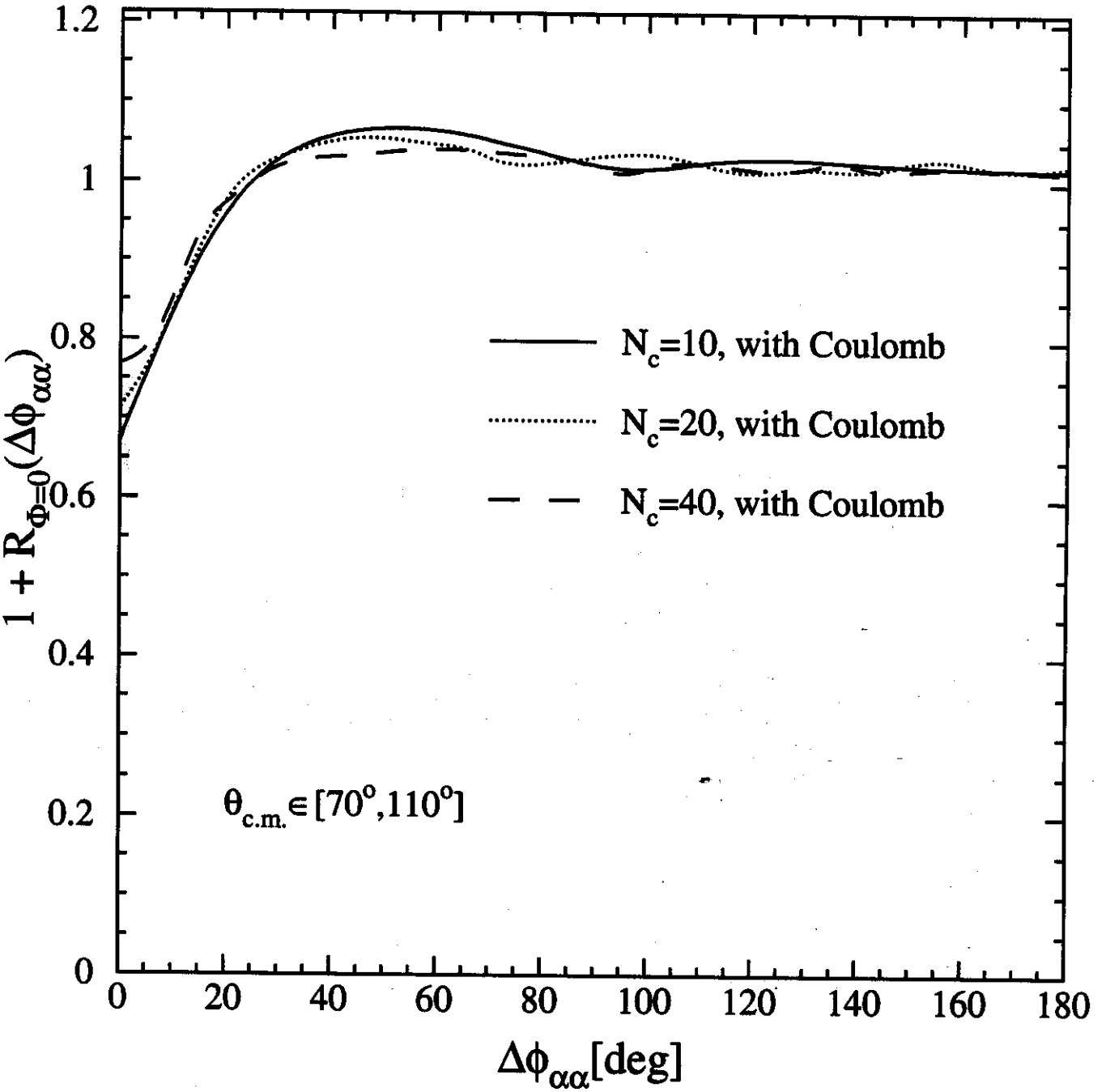
1.2
1
0.8
0.6
0.4
0.2
0
0
20
40
60
80
100
120
140
160
180
$1 + R_{\Phi=0}(\Delta\phi_{\alpha\alpha})$
$\Delta\phi_{\alpha\alpha}$[deg]
N_c=10, with Coulomb
N_c=20, with Coulomb
N_c=40, with Coulomb
$\theta_{c.m.} \in [70^o, 110^o]$

Fig. 9

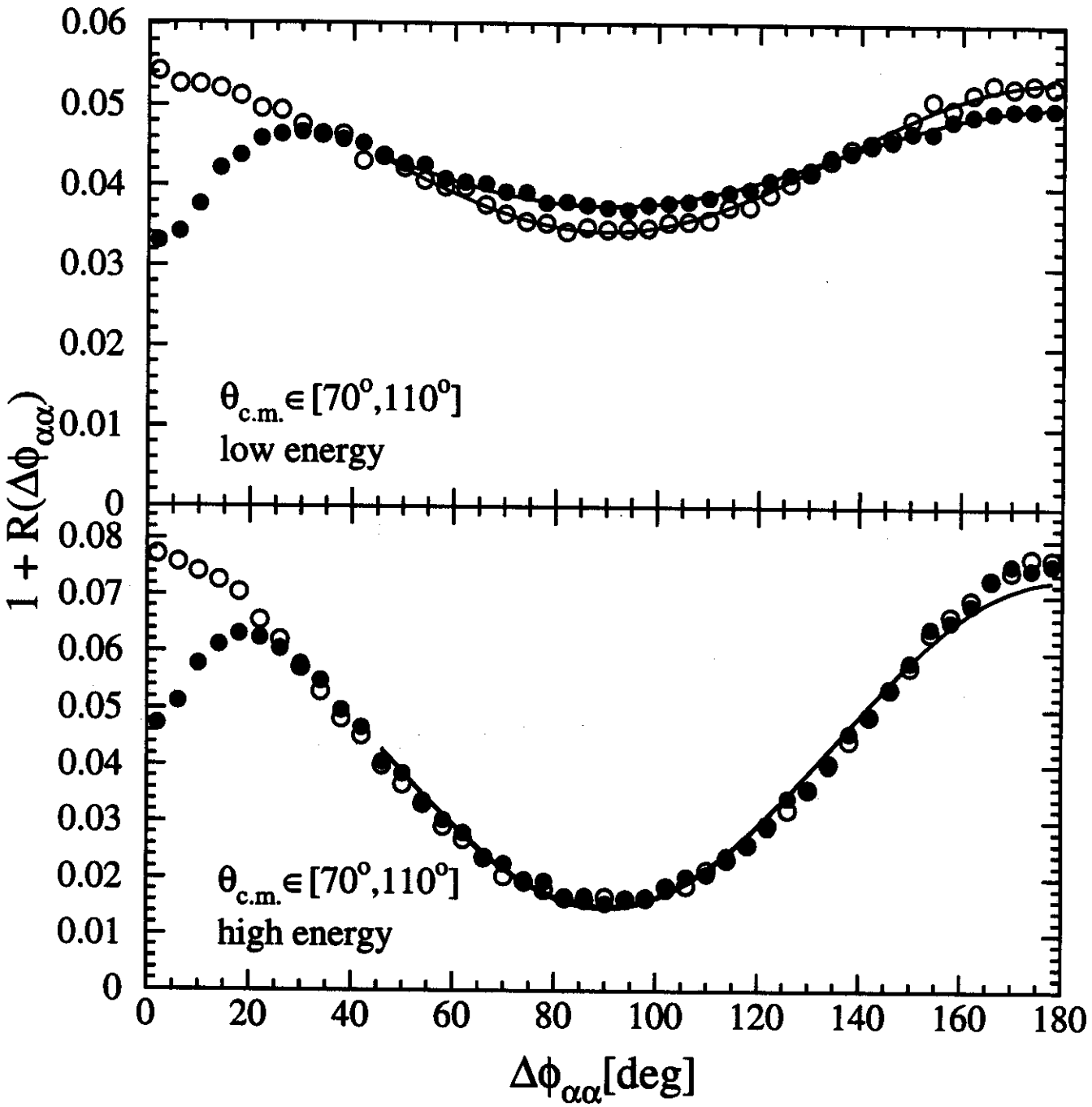
0.06
0.05
0.04
0.03
0.02
0.01
0
$\theta_{c.m.} \in [70^o, 110^o]$
low energy
0.08
0.07
0.06
0.05
0.04
0.03
0.02
0.01
0
$\theta_{c.m.} \in [70^o, 110^o]$
high energy
$1 + R(\Delta\phi_{\alpha\alpha})$
0
20
40
60
80
100
120
140
160
180
$\Delta\phi_{\alpha\alpha}$[deg]

Fig. 10

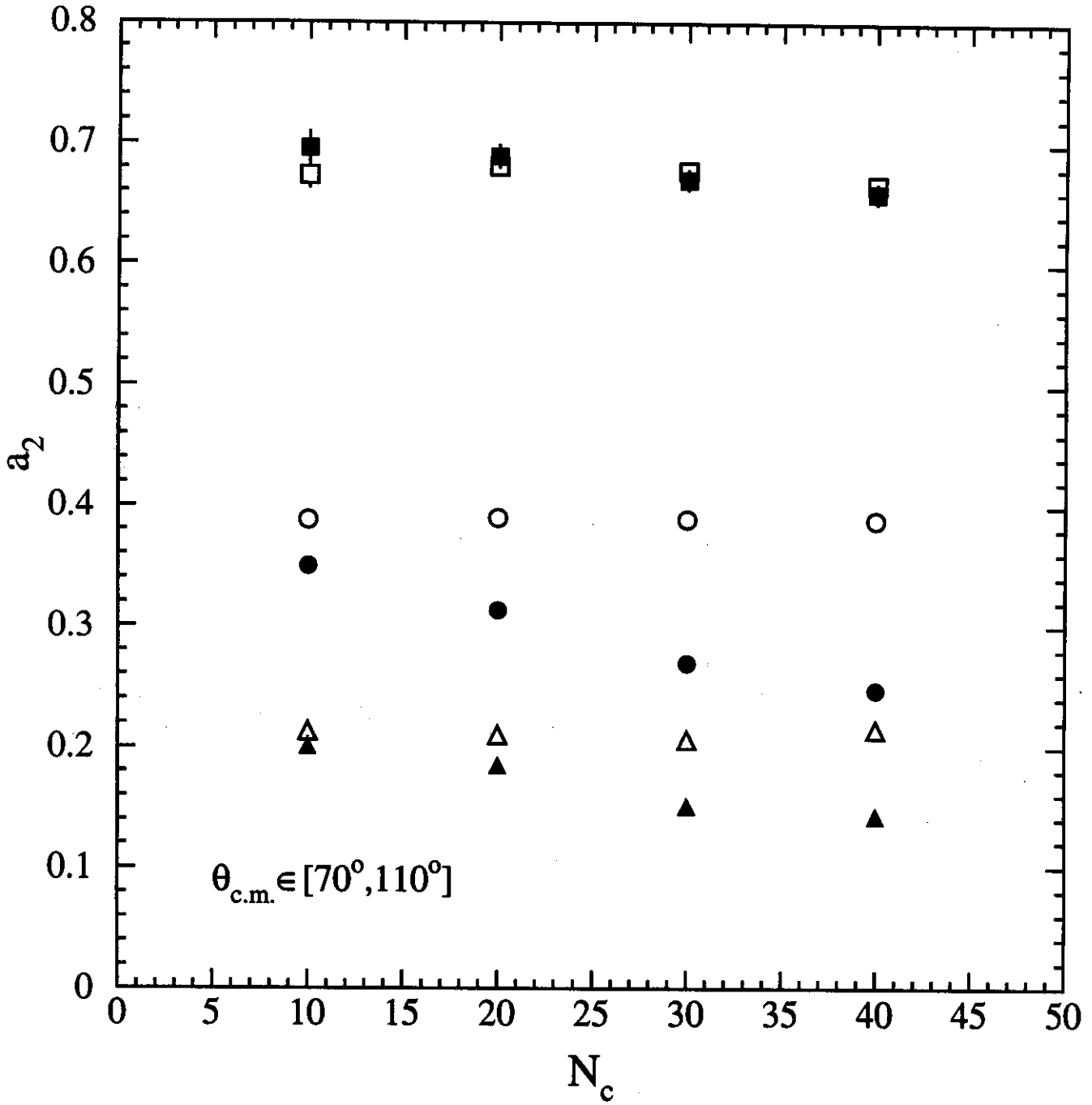
0.8
0.7
0.6
0.5
0.4
0.3
0.2
0.1
0
a_2
0
5
10
15
20
25
30
35
40
45
50
N_c
$\theta_{c.m.} \in [70^o, 110^o]$

Fig. 11